Sādhanā Vol. 32, Parts 1 & 2, February–April 2007, pp. 51–64. © Printed in India

Organised structures in wall turbulence as deduced from stability theory-based methods

P K SEN*, S V VEERAVALLI*, P W CARPENTER**, G JOSHI* and P S JOSAN*

*Dept. of Applied Mechanics, Indian Institute of Technology – Delhi, Hauz Khas, New Delhi 110 016
**School of Engineering, University of Warwick, Coventry, CV4 7AL, England
e-mail: {pksen,svrvalli}@am.iitd.ernet.in

Abstract. In earlier work, we have explored the relevance of hydrodynamic stability theory to fully developed turbulent wall flows. Using an extended Orr–Sommerfeld Equation, based on an anisotropic eddy-viscosity model, it was shown that there exists a wide range of unstable wave numbers (wall modes), which mimic some of the key features of turbulent wall flows. Here we present experimental confirmation for the same. There is good qualitative and quantitative agreement between theory and experiment. Once the dominant coherent structure is obtained from stability theory, control of turbulence would be the next logical step. As shown, the use of a compliant wall shows considerable promise.

We also present some theoretical work for bypass transition (Klebanoff/K-modes), wherein the receptivity of a laminar boundary layer to a vortex sheet in the freestream has been studied. Further, it is shown that triadic interaction between K-modes, 2D TS waves and 3D TS waves can lead to rapid algebraic growth. A similar mechanism seems to carry over to inner wall structures in wall turbulence and perhaps this is the "root cause" for sustenance of turbulence.

Keywords. Organised disturbances; hydrodynamic stability; Klebanoff modes; compliant wall.

1. Introduction

The relevance of hydrodynamic stability theory to wall-bounded turbulent flows was first extensively investigated by Reynolds and co-workers (see for example Hussain & Reynolds 1972, Reynolds & Hussain 1972). Using an eddy-viscosity model for the turbulence they derived an Orr–Sommerfeld-like equation for turbulent wall flows. However, they did not find any region of instability in their theoretical work and this was confirmed by their experiments (Hussain & Reynolds 1972).

Sen & Veeravalli (1998, 2000a) (hereinafter referred to as SV1 and SV2 respectively) considered the problem afresh and concluded that the main reason that the previous investigators failed to find any unstable modes was that they used an isotropic eddy viscosity model, which

is really not justified close to the wall. They then derived an extended Orr–Sommerfeld equation based on an anisotropic eddy viscosity model (the eddy viscosity model is similar to the one outlined in Pope 1975). The solutions, to this extended equation found by SV1, mimicked some of the key features of wall-bounded turbulent flows like the location of the production peak. Further, these modes were found to scale with inner variables and are thus universal. SV2 also noted that the dominant modes (experimentally) obtained by Hussain & Reynolds (1972), in a turbulent channel, were damped outer modes, because the disturbance frequency was too low.

The aim of the present work is to verify experimentally, the theoretical results of SV1 and SV2 and to explore the possibility of controlling turbulence with compliant walls. We also present theoretical work on the receptivity of the boundary layer (laminar) to a vortex sheet in the free stream and discuss its implications to fully turbulent wall flows by considering triadic interactions between K-modes and 2D and 3D TS waves.

2. Theory

A brief outline of the theory will be presented here (details may be seen in Sen & Veeravalli 1998, 2000) In the discussion to follow, the instantaneous velocity vector u_i and pressure p obey the incompressible Navier–Stokes and continuity equations. The velocity and pressure fields are usually decomposed in turbulent flows by the well-known Reynolds decomposition; however, here we prefer a triple decomposition as follows:

$$u_i = \bar{u}_i + \tilde{u}_i + u'_i; \quad p = \bar{p} + \tilde{p} + p'. \tag{1}$$

$\bar{u}_i$ and $\bar{p}$ are respectively the mean velocity and pressure, u'_i, p' are the (random) turbulent fluctuations and $\tilde{u}_i$, $\tilde{p}$ correspond to an organised (solenoidal) disturbance (with zero mean). The organized disturbance is assumed to be small compared to the turbulent fluctuations. After some algebra, one obtains the dynamic equation for the organised disturbance (reported in SV1). In deriving the governing equation, the disturbance stream function, ψ, is assumed to be two-dimensional and expressed as $\psi = \phi(y)e^{i\alpha(x-ct)}$, where α is the spatial wave number, and $c = c_r + ic_i$ is the complex wave speed. Note that here, as elsewhere, x, denotes the streamwise coordinate, y, the wall-normal coordinate and z, the spanwise coordinate.

In SV1 and SV2 it was shown that the unstable modes obtained are wall modes, which are found to scale perfectly with inner scales. Thus it is instructive to present the governing equation in terms of inner variables using the friction velocity u_* as the velocity scale and ν/u_* as the length scale (ν is the kinematic viscosity). We denote quantities that are non-dimensionalised by the inner scales with the superscript $(+)$. The details of the non-dimensionalisation and the physical significance of the different terms are given in SV1; here we present the final equation in inner variables:

$$\begin{aligned} &i\alpha^+[(\bar{u}^+ - c^+)(\phi'' - \alpha^{+2}\phi) - \bar{u}^{+''}\phi] - [\phi'''' - 2\alpha^{+2}\phi'' + \alpha^{+4}\phi] \\ &\quad - E^+\{\phi'''' - 2\alpha^{+2}\phi'' + \alpha^{+4}\phi\} + 2E^{+'}\{\phi''' - \alpha^{+2}\phi'\} + E^{+''}\{\phi'' + \alpha^{+2}\phi\} \\ &\quad - \lambda^+ E^+[-2i\alpha^+\phi''' + 2i\alpha^{+3}\phi'] \\ &\quad - 2i\alpha^+\phi'[\lambda^+ E^{+''} + 2\lambda^{+'}E^{+'} + \lambda^{+''}E^+] = 0. \end{aligned} \tag{2}$$

In equation (2), primes ($'$) indicate differentiation with respect to y^+. As expected the Reynolds number does not appear because of scaling with inner variables. However, the effect of the

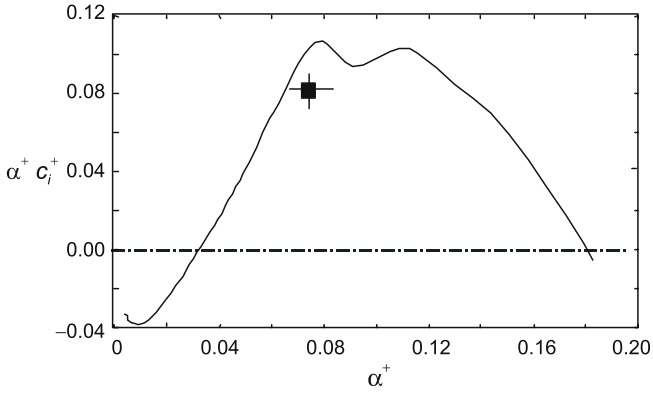

Figure 1. Growth curve $\alpha^+ c_i^+$ versus α^+ (inner variable scaling), Reynolds number (R_C) for channel flow is 5000. The curve is from SV2. The solid square is from present experiments. The lines attached to the experimental point indicate error bars.

Reynolds number is indirectly felt through the outer dependence of the non-dimensional eddy viscosity E^+, and the anisotropy function λ^+. (For details of the behaviour of E^+ and λ^+ see SV1 and SV2.). In (2), the first line corresponds to the classical Orr–Sommerfeld equation. The terms on the second line are due to the standard (isotropic) eddy viscosity model (c.f. the Newtonian eddy model of Reynolds & Hussain 1972) and the terms on the third and fourth lines correspond to the anisotropic extension to the eddy-viscosity model along the lines of Pope (1975). The anisotropy function, λ^+, may also be viewed as the reciprocal of Townsend's structure parameter (see SV1 for details).

Having formulated the stability equation, we next look at the boundary conditions for channel and boundary-layer flows. For a rigid wall, the normal velocity component vanishes at the wall, and this gives the first boundary condition. The second boundary condition is obtained from the 'no-slip' condition. Two more boundary conditions may be written in the outer region (boundary-layer edge/channel centre). In reality, it has been shown by Sen *et al* (2006) that the outer boundary condition can be obtained from the solution of the Rayleigh equation for $y > 0{\cdot}3$, for all cases of wall turbulence, where y is scaled by the outer length scale.

Figure 1 shows the solution of (2). We see that a wide range of unstable wave numbers ($\alpha^+ = 0{\cdot}03$ to $\alpha^+ 0{\cdot}18$) exists. The curve is virtually identical for boundary-layer and channel flows. It is also insensitive to the location at which the outer boundary condition is applied provided it is larger than one-third the boundary-layer thickness (or channel height). This agrees very well with the physics of high-Reynolds-number wall flows. Several other features, like the location of the production peak, agree well with standard measurements.

In case of the compliant wall, the normal velocity components from fluid side and solid side are equated. Further, the resultant velocities for the tangential no-slip conditions at the interface are also equated. Both these conditions are appropriately combined to give the first boundary condition. The second boundary condition is found by equating admittance (defined as normal wall velocity divided by pressure acting on the wall) from the fluid side (Y) and to that of solid side (Y_0). Details may be seen in Sen & Arora (1988).

3. Experiments

Measurements were made in a 2D channel specially designed for the purpose of this experiment. The half-width of the channel, H, is 0·04 m, the spanwise extent, 1·08 m and the test section is 12·2 m long. The walls (vertical) of the tunnel are made of 12 mm thick float glass

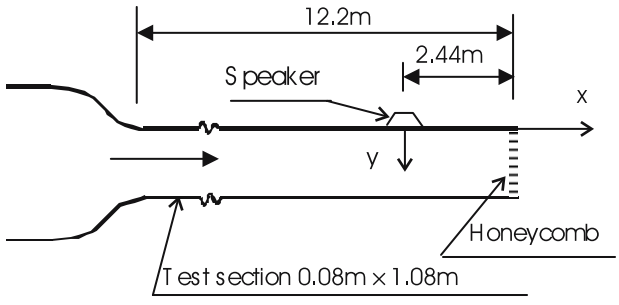

Figure 2. Schematic diagram of the setup used for experiments, showing the location of the speaker and the coordinate system in use.

(each piece 1·22 m by 2·44 m). A 4·8:1, 2D contraction, followed by a small diverging section (to ensure rapid transition) is present upstream of the test section. The organized disturbance is generated by a speaker and introduced into the flow through a slot of 1mm width and 0·15 m length, centred in the spanwise direction. A schematic diagram of the set-up and the coordinate system used is shown in figure 2.

Pressure measurements were made with a Debro micromanometer (resolution 0·01 mm) and velocity measurements were made with a boundary-layer hot-wire probe (5 μm diameter) connected to a Dantec 56C17 hot-wire anemometer and 56N20 signal conditioner. The probe position with respect to the wall was measured with the help of a travelling telescope fitted with a dial gauge of 1 μm resolution. The traverse mechanism used to move the probe was fitted with a digital Vernier calliper of 0·01 mm resolution. Using this arrangement the distance of the probe from the wall could be measured to an accuracy of 0·01 mm. Since the wire is at least 0·1 mm away from the wall in all the measurements, this accuracy is adequate.

Great care was taken to ensure that the set-up is adequately conditioned for stability work in a turbulent environment. The development length prior to the introduction of the organized disturbance is 244 H and the aspect ratio of the test section is 27. These values are large enough to ensure that well upstream of the speaker there is fully developed turbulent flow and that it remains two-dimensional in the central region (greater than 0·4 m), throughout the test section (c.f. Hussain & Reynolds 1975). The flow quality in the set-up was carefully tested, especially in the vicinity of the slot. We note that skin friction measured here agreed to within 0·5% with the data reported in Hussain & Reynolds (1975). The two-dimensionality of the disturbance at the exit of the slot and further downstream was also carefully checked and found to be satisfactory.

For the measurements being reported here, the average velocity was maintained at approximately 5·3 m/s, which corresponds to a Reynolds number of 13,200, based on the half-width of the channel. The friction velocity u_* was measured to be 0·28 m/s. Phase averages have been obtained over 11,000 cycles at each location.

In keeping with the theory presented above, the organised disturbance $\tilde{u}$, may be expressed as:

$$\tilde{u} = \frac{1}{2}\{\breve{u}(y)e^{\iota\alpha(x-ct)} + \text{c.c.}\} \tag{3}$$

where, $\breve{u}(y)$ is the eigenmode and the rms value is denoted by $\hat{u}(y)$. In theoretical work, α is usually taken to be real and the complex wave speed c is obtained as an eigenvalue. Positive c_i thus indicates instability. However, in experiments, it is the circular frequency $\beta = \alpha c$ that is real and both α and c are complex. Thus, in the experiments, the spatial growth rate is given by $-\alpha_i$ and the equivalent temporal growth rate is $-\alpha_i c_{gr}$, where, c_{gr}

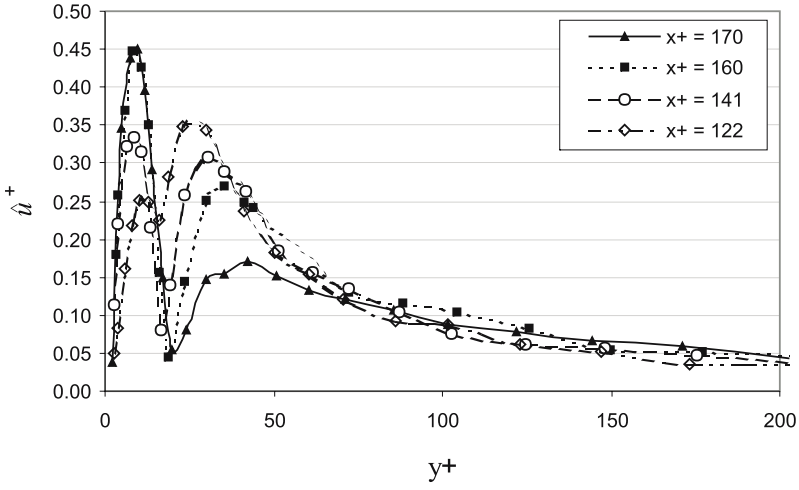

Figure 3. Evolution of the normalized rms value of the disturbance $\hat{u}^+$, with distance from the slot. The speaker frequency has been set at 300 Hz which corresponds to $\beta+ = 0{\cdot}385$. The distance from the slot has been specified in wall units in the legend and it corresponds to a variation from 7 to 10 mm.

is the group velocity. However, our calculations show that the wave speed is nearly constant over the range of wave numbers of interest; thus, the group velocity is the same as the phase velocity. Hence, the equivalent temporal growth rate in the experiments may be estimated as $\alpha_i c_r$.

Figure 3 shows the evolution of the rms of the organised disturbance $\hat{u}^+$, non-dimensionalised by inner variables. The speaker was excited at a frequency of 300 Hz, which corresponds to $\beta^+ = 0{\cdot}4$. This value was chosen so as to be close to the most unstable wave according to SV2. The four locations ($x = 7, 8, 9$ and 10 mm) shown here, correspond to an x^+ range of approximately 120–170. The data clearly show that the inner peak grows rapidly between $x = 7$ and 9 mm after which it appears to saturate. Beyond $x = 10$ mm, the eigenmode is found to decay (results not shown here), with the inner peak moving outwards. The eigenfunction (especially at $x = 10$ mm) matches the calculations of SV1 and SV2 quite well both qualitatively and quantitatively. The fact that the secondary (outer) peak reduces as we proceed from $x = 7$ to 10 mm, is probably indicative of a competition between two modes initially, a growing inner mode and a decaying outer mode. Typical results of the calculations for channel flow are shown in figure 4, where, $\hat{u}^+$ and $\hat{v}^+$ are reported for a wave number close to that of the experiments. The vertical scale in figure 4 is arbitrary and has been chosen to permit easy comparison with the experimental results. The peaks in the calculations are a little closer to the wall as compared to the experimental peaks; however, the ratio of the two peaks is very close to that observed in the experiment at $x = 10$ mm. We also note that the tail of the experimental eigenfunction is much longer, possibly due to interference from the outer mode. The location of the minimum at $y^+ \approx 20$ and the phase jump of π in the vicinity of this minimum agree well with the theoretical predictions of SV1 and SV2. The recent DNS work of Kim & Sung (2006) also shows the presence of eigenmodes similar to those observed in our experiments.

Figure 5 shows the evolution of the inner peak in the experiments. One observes a period of rapid growth followed by a somewhat slower decay. From the figure, both growth and decay

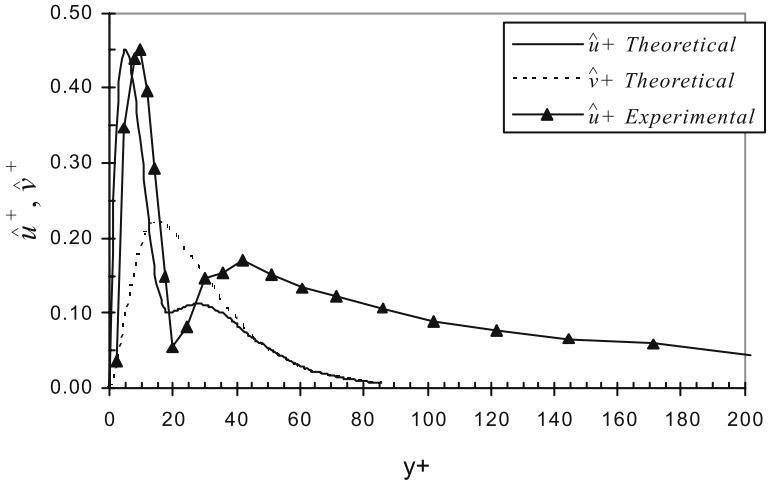

Figure 4. Comparison of calculated eigenfunctions with experiments. Calculated rms values ($\hat{u}^+$ theoretical and $\hat{v}^+$ theoretical) for channel flow at a Reynolds number of 5000. $\alpha^+ = 0{\cdot}057$; $c_r^+ = 5{\cdot}39$ and $c_i^+ = 1{\cdot}05$. Experimental ($\hat{u}^+$ experimental) values are for channel flow at a Reynolds number of 13,200. The speaker was excited with a 7 V amplitude sine wave at 300 Hz.

appear to be exponential. From the growth of the inner peak and the phase of the eigenmode, we can estimate α and c as: $\alpha_i^+ = -0{\cdot}015$; $\alpha_r^+ = 0{\cdot}074$; $c_i^+ = 1{\cdot}07$; and $c_r^+ = 5{\cdot}3$. If this is compared with the results of SV2 it is found that the data point obtained here falls almost on the $\alpha^+ c_i^+$ vs. α^+ curve. This can be seen in figure 1, where the experimental point is shown as a solid square. Such a remarkable match led us to conclude that the growth phase is indeed exponential and according to the theory presented in SV1 and SV2, and that this growth is followed by nonlinear saturation and decay. However, when the measurements were repeated with a smaller disturbance amplitude (results not shown here) the point of saturation was observed to be approximately the same, thereby ruling out the conjecture of nonlinear saturation. This indicates that the phenomenon is more complex than it appears at first glance. More detailed investigations are currently underway.

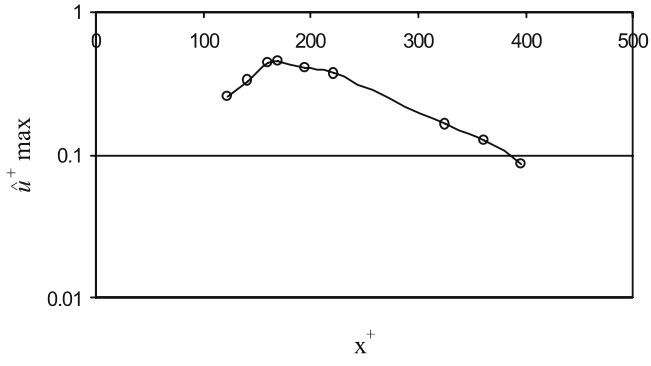

Figure 5. Evolution of the inner peak of $\hat{u}^+$ in the channel flow experiment. The disturbance frequency was set at 300 Hz.

4. Compliant wall

A detailed account of our work on the instability analysis of turbulent boundary-layer and turbulent channel flows, with compliant walls, may be found in Josan (2004) and Sen *et al* (2006). Here, we will briefly summarise the main findings. Calculations were carried out with the extended Orr–Sommerfeld equation outlined above using the inverse method of Sen & Arora (1988). Material properties for promising configurations were back-calculated using the plate spring model of Carpenter & Garrad (1985). The results show that there are two important inner 'mode classes', namely the Tollmien–Schlichting (TS) mode class and the static divergence (SD) or Kelvin–Helmholtz (KH) mode class, present in the flow. It is the TS mode class which is believed to be the so-called "root cause mechanism of turbulence", and suppression of this mode class is desirable if turbulence is to be controlled. Extensive investigations have been carried out for both the modes. It is observed that for a compliant surface with kinematic compliance, $|\bar{\phi}_w|$, greater than 70% of the corresponding freestream value of $\bar{\phi}$, the TS mode class ceases to exist, and the solution bifurcates into a high-speed highly damped (HSHD) stable mode class. Note that in the above discussion $\bar{\phi}(y)$ is the amplitude of the stream function and subscript w refers to the wall. Further, in the case of the rigid wall $|\bar{\phi}_w| = 0$. Of course, to obtain this bifurcation in the solution, the material properties of the compliant surface have to be chosen carefully. Moreover, it has been observed that, for such a surface, the SD modes do not appear. Eliminating the TS modes altogether would also result in the elimination of TS-like three-dimensional modes as well. This would result in suppression of the turbulence regeneration processes in the near-wall region. Thus, the method holds considerable promise for turbulence control.

5. Klebanoff modes

5.1 *Elucidating the vorticity source*

Both Fasel (2002) and our group (Kudar *et al* 2006 and Lockerby *et al* 2005) have been using vorticity sources derived from fictitious body forces to generate streak-like structures. Hitherto, however, we had little idea what form the vortical structures generated by these forces took. Considering, first, the simple case of a uniform flow, with this approach the governing equation for streamwise vorticity takes the form:

$$D\omega_x/Dt = Gg(y - y_s)\delta(x - x_s)F(t)\cos\beta z + \nu\nabla^2\omega_x, \tag{4}$$

where the LHS term is the material derivative; (x, y, z) are, respectively, the streamwise, wall-normal and spanwise coordinates; G is a constant source strength; (x_s, y_s) are the source coordinates; δ is a delta function; $g = \delta$ in our work but Fasel uses $g = d\delta/dy$; $F(t) = H(t) - H(t_f)$ where H is the Heaviside step function; and ν is kinematic viscosity. If viscous effects are neglected, the solution is

$$\begin{aligned} \omega_x &= Gg(y - y_s)[H(x - x_s) - H(t - x)]F(t)\cos(\beta z), \\ \omega_z &= 0. \end{aligned} \tag{5}$$

Thus, we can see that in our case of a δ function source a simple vorticity sheet is generated, which has alternating signs of vorticity in the spanwise direction. Fasel's source produces a somewhat more complex (double-δ vorticity sheet). In the case of the laminar boundary layer

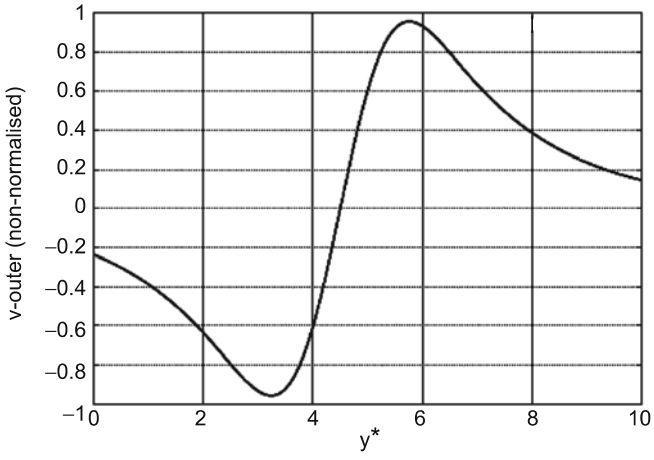

Figure 6. Un-normalised wall-normal velocity profile created in uniform flow corresponding to the Fasel (2002) double-δ vorticity source.

when the source is placed just above the edge of the boundary layer, the vortex sheet models the zero- and low-frequency streamwise vortical structures in the freestream. Kudar *et al* (2005) have shown that the laminar boundary layer is only receptive to very low-frequency streamwise vorticity and not at all to freestream spanwise vorticity.

When such a vorticity source is inserted into a turbulent boundary layer (Ali & Carpenter 2005; Lockerby *et al* 2005), the structures it generates model the hairpin vortices seen in the near-wall region. It is these that generate the sublayer streaks.

It is evident from (5) that a very strong narrow shear layer forms around $y = y_s$, so we cannot really neglect viscous effects. We can drop $\partial^2\omega_x/\partial x^2$ on the RHS of (4) because it is of higher order. For $x \gg x_s$ a quasi-self-similar steady state solution can be found that takes the form:

$$\omega_x = \hat{\Omega}(\eta)/2\nu(x - x_s); \quad \eta = (y - y_s)/\sqrt{2\nu x}. \tag{6}$$

This follows from the identity

$$\delta(y - y_s) = \exp(-\eta^2/2)/\sqrt{2\pi\nu x}, \text{ as } \nu x \to 0.$$

The Poisson relation between vorticity and stream function, namely,

$$\partial^2\psi/\partial z^2 + \partial^2\psi/\partial y^2 = -\omega_x, \tag{7}$$

is then combined with (4) and (6) to derive a fourth-order ODE for ψ that is solved numerically to give the velocity field. Figure 6 shows the (un-normalized) wall-normal velocity profile for the Fasel source.

Essentially the boundary layer is driven by the wall-normal and spanwise velocity field of the streamwise vortex sheet created by the vorticity source. A corresponding quasi-similar solution can be derived within the boundary layer, using boundary conditions at the wall; this is also required to match the uniform-flow solution. The composite wall-normal and streamwise velocity profiles are depicted in figures 7 and 8 respectively. These composite solutions agree well with the numerical-simulation results given in Fasel (2002).

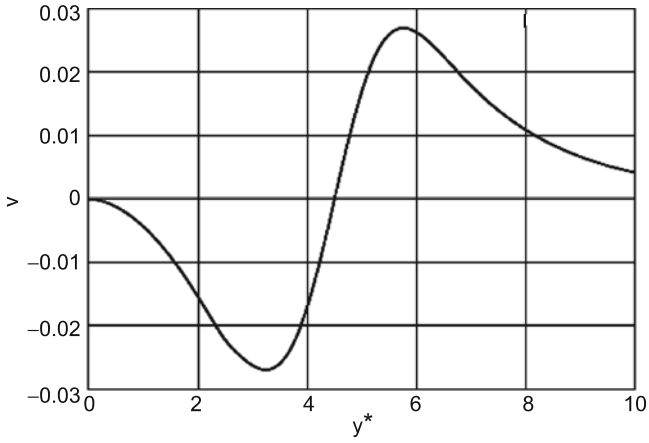

Figure 7. Composite wall-normal velocity profile corresponding to Fasel (2002).

5.2 *Nonlinear interaction between Klebanoff modes and 2D-TS waves in laminar boundary layer*

Let the flow perturbation variables be written as:

$$\phi = (u, v, w, p), \tag{8}$$

then we consider a scenario whereby

$$\phi = \phi_1 + \phi_2 + \phi_3, \tag{9}$$

where,

$$\phi_1 = \{\hat{u}_1(y), \hat{v}_1(y), \hat{p}_1(y)\} \cos \beta z; \quad \hat{w}_1(y) \sin \beta z, \tag{10}$$

corresponds to the Klebanoff mode whose solution was described above;

$$\phi_2 = \{\hat{u}_2(y), \hat{v}_2(y), \hat{p}_2(y)\} e^{i(\alpha_2 x - \omega t)}; \quad \hat{w}_2 = 0, \tag{11}$$

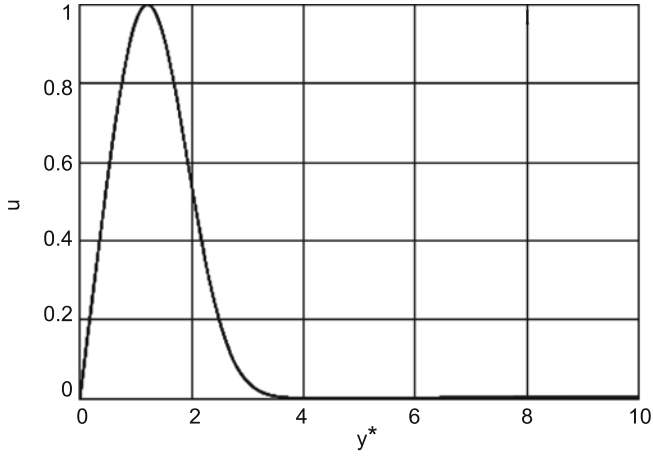

Figure 8. Composite streamwise velocity profile corresponding to Fasel (2002).

corresponds to the 2D-TS wave which we will also regard as known; and

$$\phi_3 = \{\hat{u}_3(y)\cos\beta z,\ \hat{v}_3(y)\cos\beta z,\ \hat{w}_3(y)\sin\beta z,\ \hat{p}_3(y)\cos\beta z\}\exp[i(\alpha_3 x - \omega t], \tag{12}$$

corresponds to the oblique waves generated by the nonlinear interaction between ϕ_1 and ϕ_2. The governing equation for $\hat{v}_3$ can be derived from the Navier–Stokes equations and takes the form:

$$L_{os}(\alpha_3)v_3 = \hat{R}_f e^{i(\alpha_2-\alpha_3)x}, \tag{13}$$

where, L_{os}, is the Orr–Sommerfeld operator and the forcing term

$$\hat{R}_f = [-\alpha_3\alpha_2(u_1'u_2 + u_1u_2') + i\alpha_3(u_1'v_2' + u_1''v_2) + i\alpha_2\gamma^2 u_1 v_2];$$
$$\gamma^2 = \alpha_3^2 + \beta^2. \tag{14}$$

The solution to (13) consists of the complementary function, $\tilde{v}_3$ (the solution or eigenfunction of the homogeneous equation) plus a particular solution of the form,

$$\hat{v}_{\text{total}} = x\tilde{v}_3\bar{\lambda}e^{i(\alpha_2-\alpha_3)x} + v_{3f}, \tag{15}$$

where the first term is the secular term and the second the non-secular forced solution. Equation (13) can now be written as,

$$L_3(\alpha_3)v_{3f} + \bar{\lambda}e^{i(\alpha_2-\alpha_3)x}L_2(\alpha_2)\hat{v}_3 = R_f, \tag{16}$$

where L_2 is an operator the form of which follows from the governing equation. Using the theory of adjoints as in Sen *et al* (2002, 2006) the solvability condition gives,

$$\bar{\lambda} = \int_0^\infty \theta_3\hat{R}_f\mathrm{d}y \Big/ \int_0^\infty \theta_3 L_2(\alpha_3)\tilde{v}_3\mathrm{d}y, \tag{17}$$

where θ_3 is the adjoint eigenfunction. Since R_f varies as the amplitude of the streak, $\bar{\lambda}$ is proportional to the streak strength. For weak streaks, i.e. $\bar{\lambda} \ll 1$, this only results in a correction to the eigenvalue of the form,

$$\Delta\alpha_3 = -i\bar{\lambda}e^{i(\alpha_2-\alpha_3)x}. \tag{18}$$

The difference in the real parts of the wave-numbers contributes a change of phase while the difference in imaginary parts leads to amplification or attenuation depending on its sign. This means that while propagating along the boundary layer $\Delta\alpha_3$ varies in magnitude owing both to phase and amplitude change. Hence, the effect is amplifying over short distances giving the intermittent bursting observed by Fasel (2002) in his simulations. For stronger streaks leading to large $\bar{\lambda}$, the behaviour is qualitatively different because explosive algebraic growth can exist owing to the existence of the secular solution. For example the secular part of $\hat{v}_{\text{total}}$ can be shown to behave as $x\bar{\lambda}\tilde{v}_3 e^{i(\alpha_2 x-\omega t)}$. We have demonstrated numerically that both scenarios are plausible and would expect algebraic growth to start to dominate when $u_1 \geq 0{\cdot}1U_\infty$.

A typical result for algebraic growth for a laminar damped case is given in figure 9. The spatial problem has been solved for a laminar boundary layer with the following input data

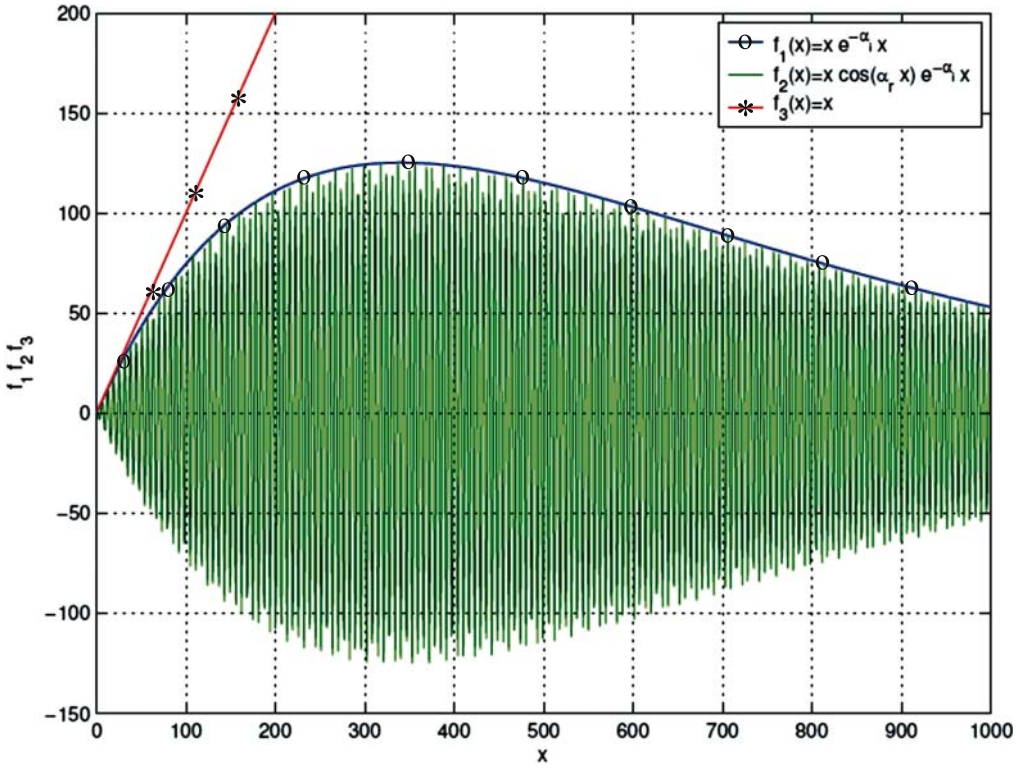

Figure 9. Algebraic growth due to K (streaks) +2D-TS + 3D-TS waves interacting for laminar damped case.

(normalised by the freestream velocity and boundary-layer thickness): $R = 1500, \omega = 0{\cdot}4, \beta = 0{\cdot}2$.

For this input we obtain eigenvalues α_2 and α_3 as:

$$\alpha_2 = 0{\cdot}48729 + i0{\cdot}002936 \text{ and } \alpha_3 = 0{\cdot}98256 + i0{\cdot}00441142.$$

Corresponding to this $|\bar{\lambda}| = 0{\cdot}15682$, figure 9 shows algebraic growth corresponding to the above parameters, plotted to a free scale for the vertical co-ordinate y. Also the x co-ordinate gives distance in x from the point of inception of algebraic growth.

The function $f_1(x) = xe^{-\alpha_i x}$ is the envelope of the algebraic growth curve, $f_2(x) = x\cos(\alpha_r x)e^{-\alpha_i x}$ shows the full function with the spatial variation in x for the parameters above. Also $f_3(x) = x$ shows the linear growth line corresponding to algebraic growth. It is seen that considerable algebraic growth occurs even though the mode is damped.

Figure 10 shows algebraic growth for an amplified turbulent mode with $R = 5000, \alpha = 31{\cdot}0$ and $\beta = 17{\cdot}90$ using the boundary-layer thickness and freestream velocity as length and velocity scales respectively.

This problem is investigated for algebraic growth in the temporal domain. The eigenvalues for the phase speeds c_2 and c_3, respectively for the 2D-TS and 3D-TS modes are given as:

$$c_2 = 0{\cdot}350975 + i0{\cdot}00559564, c_3 = 0{\cdot}300454 + i0{\cdot}00536667.$$

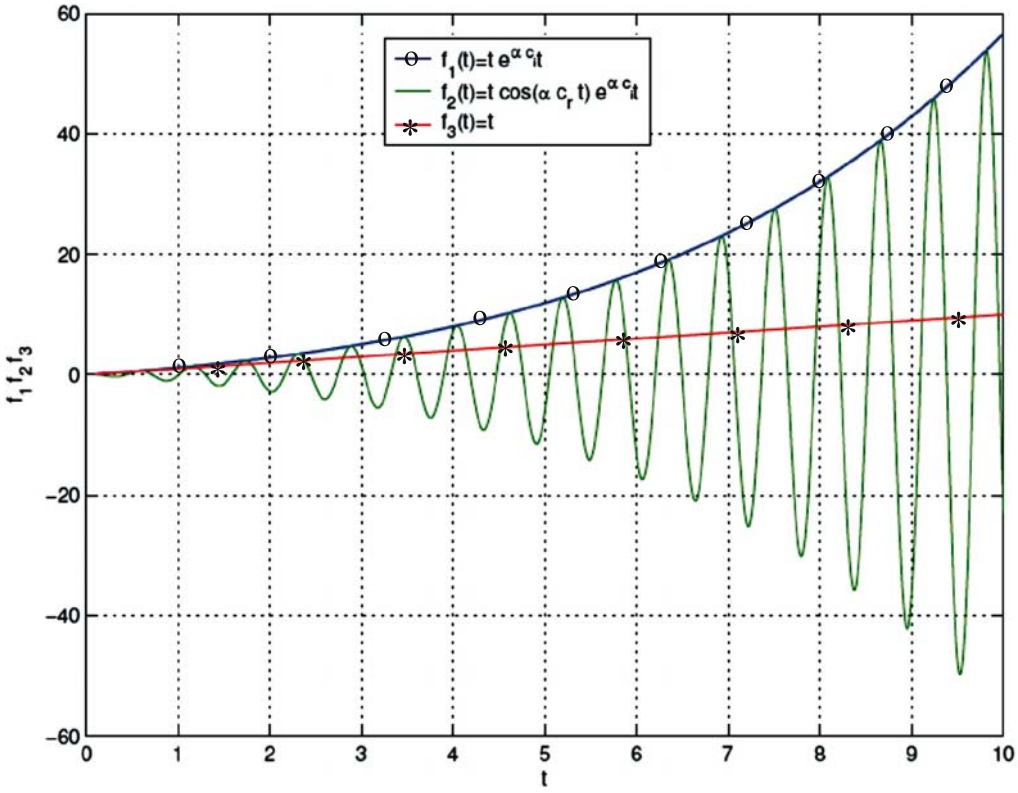

Figure 10. Preliminary results for algebraic growth due to K (streaks) +2D-TS + 3D-TS waves interacting for turbulent amplified case.

All the corresponding values in inner variables (superscripted by a (+) sign) are given as follows.

$$R^+ = 1, \alpha^+ = 0{\cdot}1088, \beta^+ = 0{\cdot}062832, c_2^+ = 6{\cdot}1581 + i0{\cdot}98180;$$

$c_3^+ = 5{\cdot}2717 + i0{\cdot}09417$. $|\bar{\lambda}|$ corresponding to this mode is 15·1838.

The growth rate αc_{2i} is given as $0{\cdot}173464t$. Since $c_{2i} > 0$, this mode is amplifying. Figure 10 shows plots again for $f_1(t) = te^{\alpha c_i t}$, $f_2(t) = t\cos(\alpha c_r t)e^{\alpha c_i t}$ and $f_3(t) = t$, as in figure 9, but this time for the temporal domain t. Clearly this figure shows algebraic growth, which is later superseded by exponential growth.

The next case is for a turbulent damped mode with $R = 5000$, $\alpha = 8{\cdot}985$, $\beta = 17{\cdot}90$. The eigenvalues for a phase speeds c_2 and c_3, respectively for the 2D-TS and 3D-TS modes are given as:

$$c_2 = 0{\cdot}282756 - i0{\cdot}00152036, c_3 = 0{\cdot}187251 - i0{\cdot}01185049.$$

All the corresponding values in inner variables are given as follows:

$$R^+ = 1; \alpha^+ = 0{\cdot}03153; \beta^+ = 0{\cdot}062832; c_2^+ = 4{\cdot}9611 - i0{\cdot}026676;$$

$c_3^+ = 3{\cdot}2854 - i0{\cdot}208531$. $|\bar{\lambda}|$ corresponding to this mode is 2·6808.

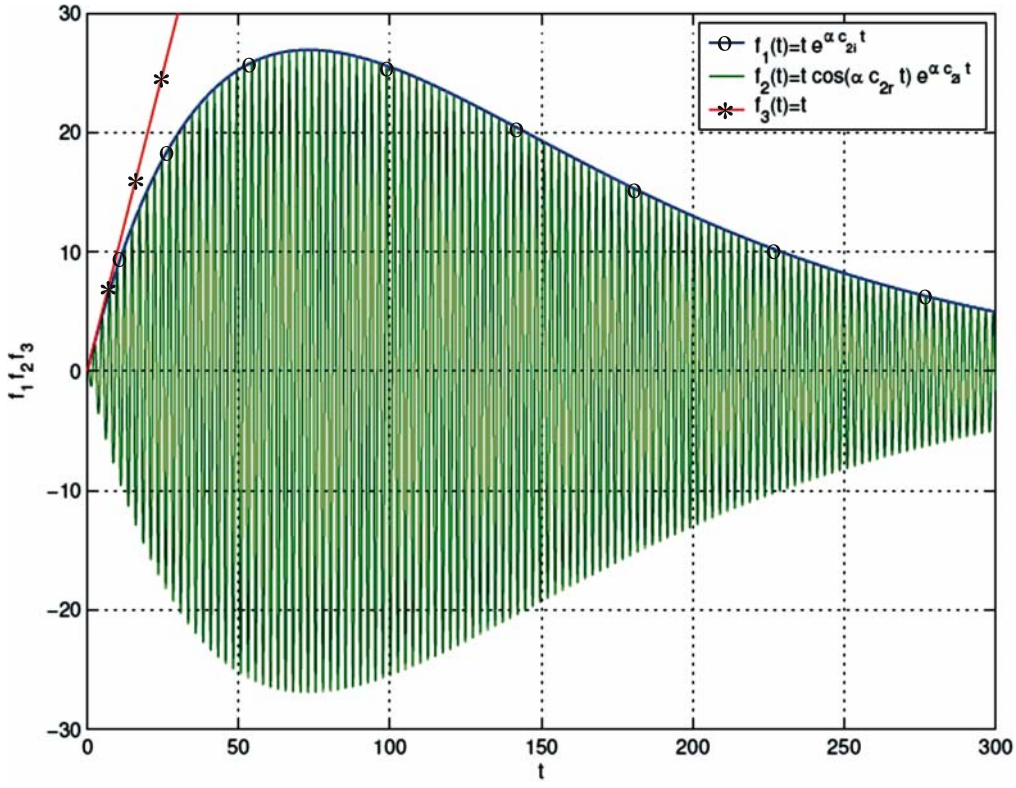

Figure 11. Preliminary results for algebraic growth due to K (streaks) +2D-TS + 3D-TS waves interacting for turbulent damped case.

In this case the mode is damped and the growth rate is given as $\alpha c_{2i} = -0{\cdot}0136572t$. Figure 11 shows considerable algebraic growth before damping takes place.

6. Conclusions

Fairly strong experimental evidence has been presented here for the theory outlined in SV1 and SV2. The shape of the eigenmode, obtained experimentally, matches the calculated eigenmode well. In the region of growth of the inner maximum, the experimentally observed wave number, wave speed, growth rate etc. are in good agreement with the theoretical values. Thus we can claim that linear stability does provide a vital clue to the mechanism of sustenance of turbulence even in wall-bounded flows.

The work on compliant walls is very promising for flow control in that it shows that with a proper choice of wall parameters the unstable TS modes can be completely eliminated. The significance of this result is strengthened by the work on K-modes and bypass transition.

We have obtained a quasi-similar solution to the vorticity and stream function equations, in the presence of freestream body force, which reproduces the DNS results of Fasel (2002) almost exactly. It has been shown further that the triadic interaction between the K-modes and 2D-TS and 3D-TS waves could lead to explosive algebraic growth. This is most probably

the mechanism of bypass transition. A similar mechanism could exist in fully developed turbulent wall flows wherein streamwise vortices in the near-wall region take the place of the freestream body force used in the laminar flow calculations. The resulting K-modes and their interaction with 2D-TS and 3D-TS modes would lead to similar explosive growth (bursting), for which preliminary results have already been obtained. Thus interfering with generation of the unstable 2D-TS waves would quench this mechanism and help in the control of turbulence in wall-bounded flows.

References

Ali R, Carpenter P W 2005 Effect of wall compliance on streak-like flow structures. *Proc. 2nd Int. Symp. on Sea-water Drag Reduction*, Busan, Korea

Carpenter P W, Garrad A D 1985 The hydrodynamic stability of flow over Kramer-type compliant surfaces Part 1. Tollmein–Schlichting instabilities. *J. Fluid Mech.* 150: 465–510

Fasel H 2002 Numerical investigation of the interaction of the Klebanoff-mode with a Tollmein–Schlichting wave. *J. Fluid Mech.* 450: 1–33

Hussain A K M F, Reynolds W C 1972 The mechanics of an organized wave in turbulent shear flow, Part 2. Experimental results. *J. Fluid Mech.* 54: 241–261

Hussain A K M F, Reynolds W C 1975 Measurements in fully developed turbulent channel flow. *J. Fluids Eng.* 97: 568–578

Josan P S 2004 *Suppression of wall turbulence using a compliant surface based on stability and turbulence analysis*, PhD thesis, Indian Inst. Technology, New Delhi

Kim K, Sung H J 2006 Effects of unsteady blowing through a spanwise slot on a turbulent boundary layer. *J. Fluid Mech.* 557: 423–450

Kudar K L, Carpenter P W, Davies C 2005 Generation of boundary-layer disturbances by freestream forcing, *Bull. Am. Phys. Soc.* 50(9): 180

Kudar K L, Carpenter P W, Davies C 2006 Klebanoff modes in swept boundary layers. In *Sixth IUTAM Symposium on Laminar-Turbulent Transition* (ed.) R Govindarajan (Springer) pp 167–172

Lockerby D A, Carpenter P W, Davies C 2005 Control of sublayer streaks using microjet actuators. *AIAA J.* 43: 1878–1886

Pope S B 1975 A more general effective viscosity hypothesis. *J. Fluid Mech.* 72: 331–340

Reynolds W C, Hussain A K M F 1972 The mechanics of an organized wave in turbulent shear flow, Part 3. Theoretical models and comparison with experiments. *J. Fluid Mech.* 54: 263–288

Sen P K, Arora D S 1988 On the stability of laminar boundary layer over a flat plate with a compliant surface. *J. Fluid Mech.* 197: 201–240

Sen P K, Josan P S, Veeravalli S V 2006 Suppression of wall turbulence based on stability and turbulence analysis using a compliant surface. In *Sixth IUTAM Symposium on Laminar-Turbulent Transition* (ed.) R Govindarajan (Springer) pp 231–236

Sen P K, Veeravalli S V 1998 On the behavior of organized disturbances in a turbulent boundary layer. *Sādhanā* 23: 167–193

Sen P K, Veeravalli S V 2000a Behavior of organized disturbances in fully developed turbulent channel flow. *Sādhanā* 25: 423–437

Sen P K, Veeravalli S V 2000b Hydrodynamic stability theory and wall turbulence. *Curr. Sci.* 79: 840–848

Sen P K, Hegde S, Carpenter P W 2002 Simulation of small disturbance waves over alternate rigid and compliant panels, *Indian J. Eng. Mat. Sci.* 9: 409–413